

New Aspects of Geometric Phases in Experiments with polarized Neutrons

S. Sponar¹, J. Klepp², K. Durstberger-Rennhofer¹, R. Loidl¹, S. Philipp³, M. Lettner⁴, R. A. Bertlmann², G. Badurek¹, H. Rauch^{1,5} and Y. Hasegawa¹

¹ Atominstitut der Österreichischen Universitäten, TU-Wien, 1020 Vienna, Stadionallee 2, Austria

² Faculty of Physics, University of Vienna, Boltzmanngasse 5, 1090 Vienna, Austria

³ Department of Physics, ETH Zürich, Schafmattstr. 16, 8093 Zürich, Switzerland

⁴ Max-Planck-Institut für Quantenoptik, Hans-Kopfermann-Straße 1, 85748 Garching, Germany

⁵ Institut Laue-Langevin, B.P. 156, 38042 Grenoble Cedex 9, France

E-mail: sponar@ati.ac.at

Abstract. Geometric phase phenomena in single neutrons have been observed in polarimeter and interferometer experiments. Interacting with static and time dependent magnetic fields, the state vectors acquire a geometric phase tied to the evolution within spin subspace. In a polarimeter experiment the non-additivity of quantum phases for mixed spin input states is observed. In a Si perfect-crystal interferometer experiment appearance of geometric phases, induced by interaction with an oscillating magnetic field, is verified. The total system is characterized by an entangled state, consisting of neutron and radiation fields, governed by a Jaynes-Cummings Hamiltonian. In addition, the influence of the geometric phase on a Bell measurement, expressed by the Clauser-Horne-Shimony-Holt (CHSH) inequality, is studied. It is demonstrated that the effect of geometric phase can be balanced by an appropriate change of Bell angles.

PACS numbers: 03.75.Dg, 03.65.Vf, 03.65.Ud, 07.60.Ly, 42.50.Dv, 03.75.Be

Submitted to: *J. Phys. A: Math. Gen.*

1. Introduction

The total phase acquired during an evolution of a quantum system generally consists of two components: the usual dynamical phase ϕ_d and the geometric phase ϕ_g . The dynamical phase, which depends on the dynamical properties, like energy or time is given by $\phi_d = -1/\hbar \int H(t)dt$. The peculiarity of the geometric phase lies in the fact that it does not depend on the dynamics of the system, but purely on the evolution path of the state. Considering a spin $\frac{1}{2}$ system, the geometric phase is given by minus half the solid angle ($\phi_g = -\Omega/2$) of the curve traced out. Since its discovery by M. V. Berry in 1984 [1] the topological concept has been widely expanded and has undergone several generalizations.

The first experimental evidence of an adiabatic and cyclic geometric phase, commonly called Berry phase, was achieved with photons in 1986 [2] and later with neutrons [3]. Non-adiabatic [4] and non-cyclic [5] geometric phases as well as the off-diagonal case, where initial and final states are mutually orthogonal [6], have been considered. In addition to an early approach by Uhlmann [7], an alternative concept of geometric phase for mixed input states based on interferometry was developed by Sjöqvist *et al.* [8]. Here, each eigenvector of the initial density matrix independently acquires a geometric phase. The total mixed state phase is a weighted average of the individual phase factors. This concept is of great significance for all experimental situations or technical applications in which pure state theories oversimplify the description. Theoretical predictions have been tested using NMR and single-photon interferometry [9, 10]. The idea has also been extended to the off-diagonal case [11, 12].

Neutron interferometry [13, 14] provides a powerful tool for investigations of quantum phenomena. Particularly in the field of geometric phases, where the spatial as well as the spinor evolution leads to geometric phases: In the spatial case the two-dimensional Hilbert space is spanned by the two possible paths in the interferometer. It has been experimentally verified that a geometric phases for cyclic [15], as well as non-cyclic evolutions [16], can be induced. In the case of spinor evolution, where the geometric phase is generated in spin subspace, the spinor rotations are carried out independently in each sub-beam, due to the macroscopic separation of the partial beams in the interferometer [17]. Geometric phase effects are observed when the two sub-beams are recombined at the third plate of the interferometer followed by a spin analysis. For instance in [18], spin flippers in both beams clearly demarcate the separate contributions of the dynamical and geometric phase acquired in the spin subspace.

The geometric phase in a single-particle system has been studied widely over the past two and a half decades. Nevertheless its effect on entangled quantum systems is less investigated. The Berry phase is an excellent candidate to be utilized for logic gate operations in quantum communication [19], due to its robustness against noise. This has been tested recently using superconducting qubits [20], and trapped polarized ultracold neutrons [21]. Entanglement is the basis for quantum communication and quantum information processing. Therefore studies on systems combining both quantum

phenomena, the geometric phase and quantum entanglement, are of great importance [22, 23, 24]. In the case of neutrons, entanglement is achieved between different degrees of freedom and not between different particles. Using neutron interferometry, with spin polarized neutrons, single-particle entanglement between the spinor and the spatial part of the neutron wave function [25], as well as full tomographic state analysis [26], have already been accomplished.

In this paper we report on miscellaneous geometric phase phenomena in neutron polarimetry as well as interferometry. In Section 2 polarimetric measurements of noncyclic geometric, dynamical and general phases are presented. In particular, our experiment demonstrates that the geometric and dynamical mixed state phases Φ_g and Φ_d , resulting from separate measurements, are not additive [28] in the sense that the total phase resulting from a single, cumulative, measurement differs from $\Phi_g + \Phi_d$ [29, 30]. Furthermore, we report on observation and manipulation of the geometric phase generated in one of the Hilbert spaces in a spin-path entangled single neutron system, namely the spin subspace. Section 3 focuses on the geometric phase generation, due to time-dependent interaction with a radio-frequency (rf) field. Here the system is characterized by an entangled state, consisting of neutron and radiation field, governed by a Jaynes-Cummings Hamiltonian. In Section 4 the influence of the geometric phase on a spin-path entangled single neutron system is described. We demonstrate in detail how the geometric phase affects the Bell angle settings, required for a violation of a Bell-like inequality in the CHSH formalism.

2. Experimental observation of non-additivity of mixed-state phases

2.1. Neutron polarimeter scheme for phase measurement

Consider the experimental setup shown in Fig. 1. The polarizer P prepares the beam in the $|\uparrow\rangle$ spin state. Subsequently, a coil carries out a $\pi/2$ -rotation (U_1), creating a coherent superposition $1/\sqrt{2}(|\uparrow\rangle - i|\downarrow\rangle)$ of spin eigenstates that acquire opposite dynamical phase due to Zeeman splitting within the field B_z . Alternatively, one could say that the polarization vector \vec{r}' rotates in the x, y plane after U_1 . The second coil and some arbitrarily chosen propagation distance within B_z implement a spin evolution U_ϕ for both eigenstates and thereby induces a pure state Pancharatnam (total) phase ϕ [31]. The third coil (U_1^\dagger) carries out a $-\pi/2$ -rotation in order to observe spin interference in the detector D after the analyzer A (both, P and A project the spin towards the $+z$ direction). To obtain these interferences a phase shift η is implemented by linear translation of the second coil. It was first stated in [32] that with such an apparatus one can obtain phases ϕ between spin eigenstates of neutrons, induced by a $SU(2)$ transformation

$$U_\phi(\xi, \delta, \zeta) = e^{i\delta} \cos \xi |\uparrow\rangle\langle\uparrow| - e^{-i\zeta} \sin \xi |\uparrow\rangle\langle\downarrow| + e^{i\zeta} \sin \xi |\downarrow\rangle\langle\uparrow| + e^{-i\delta} \cos \xi |\downarrow\rangle\langle\downarrow|. \quad (1)$$

Equation (1) describes a general evolution of the system within static magnetic fields. The resulting total phase $\phi = \arg\langle\uparrow|U_\phi|\uparrow\rangle = \delta$ can be written as a function of the

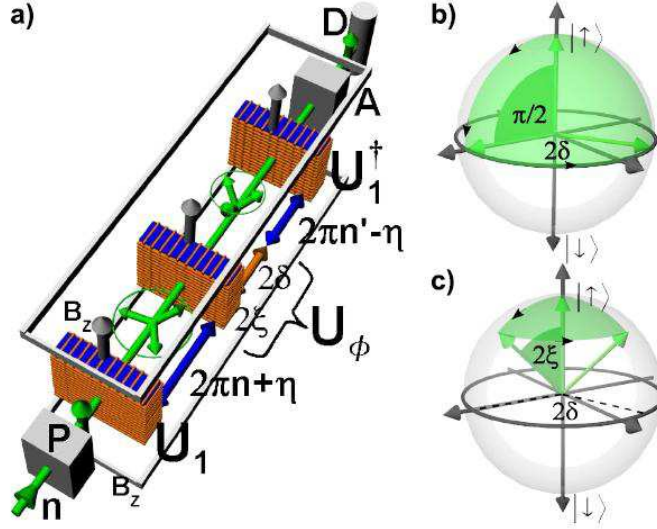


Figure 1. a) Sketch of neutron polarimetry setup for phase measurement with overall guide field B_z , polarizer P , three DC-coils to implement unitary operations U_1 , U_1^\dagger , U_ϕ , analyzer A and detector D . Greek letters denote polarization rotation angles. Shifting the second coil induces an additional dynamical phase $\eta/2$ resulting in spin interference. Evolution of the $|\uparrow\rangle$ state on the Bloch-sphere induced by U_ϕ , associated to: b) Purely (noncyclic) geometric phase ($2\xi = \pi/2$). c) Combinations of dynamical and geometric phase on the Bloch sphere ($0 < 2\xi < \pi/2$).

maximum I_{max} and minimum I_{min} intensity of the oscillations, exhibited by applying the phase shift η . The intensity is proportional to $\cos^2 \xi \cos^2 \delta + \sin^2 \xi \cos^2(\zeta - \eta)$. This only depends on the SU(2) parameters ξ , δ and ζ - set by choosing the spin rotation angles in the second coil and the additional propagation distance within the guide field B_z , respectively.

A neutron beam with incident purity $r' = |\vec{r}'|$ along the $+z$ -axis ($\vec{r}' = (0, 0, r')$) is described by the density operator $\rho_{in}(r) = 1/2(\mathbb{1} + r'\sigma_z)$. For mixed input states, $0 \leq r' < 1$. In this case [33] we find the intensity oscillations to be proportional to

$$I^\rho = \frac{1 - r'}{2} + r' (\cos^2 \xi \cos^2 \delta + \sin^2 \xi \cos^2(\zeta - \eta)). \quad (2)$$

Considering again the maxima and minima of the intensity oscillations, one obtains the mixed state phase

$$\Phi(r') = \arccos \sqrt{\frac{[I_{min}^\rho/I_n^\rho - 1/2(1 - r')]/r'}{r'[1/2(1 + r') - I_{max}^\rho/I_n^\rho] + [I_{min}^\rho/I_n^\rho - 1/2(1 - r')]/r'}} \quad (3)$$

with a normalization factor $I_n^\rho = 2I_0^\rho/(1 + r')$. I_0^ρ is the intensity measured with $U_\phi = \mathbb{1}$.

Generally, the noncyclic geometric phase is given by $\phi_g = -\Omega/2$, where Ω is the solid angle enclosed by an evolution path and its shortest geodesic closure on the Bloch sphere [5]: ϕ_g and the total phase ϕ are related to the path by the polar and azimuthal angles 2ξ and 2δ respectively, so that the pure state geometric phase can be written as

$$\phi_g = \phi - \phi_d = \delta[1 - \cos(2\xi)]. \quad (4)$$

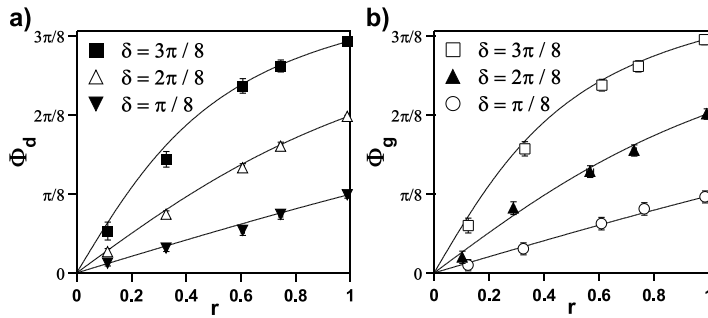


Figure 2. Mixed state phases determined from measured intensity oscillations using Eq.(5). Dynamical phase (a), geometric phase (b) versus input purity r for three evolution paths, i. e. three settings of the second coil (angle 2ξ) and flight distance after it (angle 2δ). The legends indicate evolutions. Solid lines are theory curves using the rightmost data points as reference.

ϕ_d is the dynamical phase. By proper choice of 2ξ and 2δ , U_ϕ can be set to generate purely geometric, purely dynamical, or arbitrary combinations of both phases, e.g. in Figs.1b and c: For instance, we can choose to induce a purely geometric phase by selecting 2ξ to be equal to $\pi/2$.

The theoretical prediction for the mixed state phase is [8, 33]

$$\Phi = \arctan(r' \tan \delta) \quad (5)$$

Note that Eq. (5) only depends on the parameter δ and the purity r' . Again, as can be seen also from Eq. (4), the parameter ξ only determines the portion of dynamical phase ϕ_d contained in the total phase ϕ .

2.2. Experiment

To access Eq. (5) experimentally r' has to be varied. In addition to the DC current, which effects the transformation U_1 , random noise is applied to the first coil, thereby changing B_x in time. Neutrons, which are part of the ensemble $\rho_{in}(r')$, arrive at different times at the coil and experience different magnetic field strengths. We are left with the system in a mixed state $\vec{r}=(0, -r, 0)$ where $r < 1$ [34].

A neutron beam – incident from a pyrolytic graphite crystal – with a mean wavelength $\lambda \approx 1.98 \text{ \AA}$ and spectral width $\Delta\lambda/\lambda \approx 0.015$, was polarized up to 99% by reflection from a bent Co-Ti supermirror array. The final maximum intensity was about 150 counts/s at a beam cross-section of roughly 1 cm^2 . A ^3He gas detector was used. Spin rotations around the $+x$ -axis were implemented by magnetic fields B_x from DC coils on frames with rectangular profile ($7 \times 7 \times 2 \text{ cm}^3$). B_z was realized by two rectangular coils of 150 cm length in Helmholtz geometry. Low coil currents of about 2 A corresponding to field strengths of up to 1 mT were required for the spin rotations and to prevent unwanted depolarization. The noise from a standard signal generator consisted of random DC offsets varying at a rate of 20 kHz. The experimental data

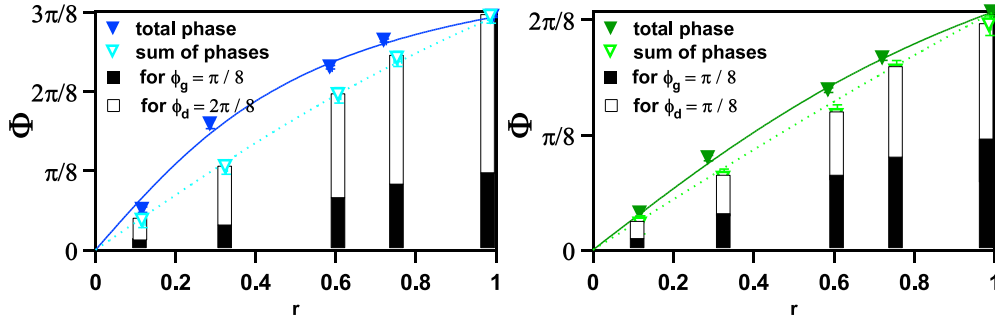


Figure 3. Filled markers: Measured total mixed state phase Φ_{tot} versus purity r for two examples of U_{tot} associated to the total pure state phases $\phi_g + \phi_d$ (see text). Open markers: $\Phi_g + \Phi_d$ as calculated from measured data. Filled (empty) bars show measured mixed-state geometric (dynamical) phases. The solid and dotted theory curves assume either non-additivity or additivity, respectively.

shown in Fig. 2 reproduce well the r' -dependence predicted by Eq. (5).

2.3. Non-additivity

Our experiment focuses on a special property of the mixed state phase: its non-additivity. The Sjöqvist mixed state phase [8] is defined as a weighted average of phase factors rather than one of phases. So it is true only for pure states that phases accumulated in separate experiments can be added up to the usual total phase in the following sense: Suppose a geometric pure state phase ϕ_g is induced in a first, and a dynamic pure state phase ϕ_d in a second measurement. Applying (4) we can also choose a combination of angles 2ξ and 2δ leading to a transformation U_{tot} , so that we measure the total pure state phase $\phi_g + \phi_d$ in a third experiment. However, the result of this latter experiment for the system initially in a mixed state is $\Phi_{tot}(r) = \arctan[r \tan(\phi_g + \phi_d)]$. The total phase is *not* equal to $\Phi_g(r) + \Phi_d(r)$, with $\Phi_g(r) = \arctan(r \tan \phi_g)$ and $\Phi_d(r) = \arctan(r \tan \phi_d)$. Two examples of data confirming this prediction are shown in Fig. 3.

3. Geometric phase generation in an oscillating magnetic field

The evolution of a system consisting of neutron, static magnetic field and quantized rf-field can be described by a photon-neutron state vector, which is an eigenvector of a Jaynes-Cummings (J-C) Hamiltonian [35, 36], adopted for this particular physical configuration [37]. Since two rf-fields (the reason for the second rf-field is explained in Section 3.1), operating at frequencies ω and $\omega/2$, are involved in the actual experiment, the modified corresponding J-C Hamiltonian is denoted as

$$\mathcal{H}_{J-C} = -\frac{\hbar^2}{2m} \nabla^2 - \mu B_0(\mathbf{r}) \sigma_z + \hbar(\omega a_\omega^\dagger a_\omega + \frac{\omega}{2} a_{\omega/2}^\dagger a_{\omega/2}) \quad (6)$$

$$+ \mu \left(\frac{B_1^{(\omega)}(\mathbf{r})}{\sqrt{N_\omega}} (a_\omega^\dagger \tilde{\sigma} + h. c.) + \frac{B_1^{(\omega/2)}(\mathbf{r})}{\sqrt{N_{\omega/2}}} (a_{\omega/2}^\dagger \tilde{\sigma} + h. c.) \right). \quad (7)$$

with $\tilde{\sigma} = \frac{1}{2}(\sigma_x + i\sigma_y)$. The first term accounts for the kinetic energy of the neutron. The second term leads to the usual Zeeman splitting of $2|\mu|B_0$. The third term adds the photon energy of the oscillating fields of frequencies ω and $\omega/2$, by use of the creation and annihilation operators a^\dagger and a . Finally, the last term represents the coupling between photons and the neutron, where $N_{\omega_j} = \langle a_{\omega_j}^\dagger a_{\omega_j} \rangle$ represents the mean number of photons with frequencies ω_j in the rf-field.

The state vectors of the oscillating fields are represented by coherent states $|\alpha\rangle$, which are eigenstates of a^\dagger and a . The eigenvalues of coherent states are complex numbers, so one can write $a|\alpha\rangle = \alpha|\alpha\rangle = |\alpha|e^{i\phi}|\alpha\rangle$ with $|\alpha| = \sqrt{N}$. Neutrons interacting with electromagnetic quanta are usually described by the 'dressed-particle' formalism [37], in analogy to the dressed-atom concept [38] developed nearly two decades before. Using Eq. (7) one can define a total state vector including not only the neutron system $|\Psi_N\rangle$, but also the two quantized oscillating magnetic fields:

$$|\Psi_{\text{tot}}\rangle = |\alpha_\omega\rangle \otimes |\alpha_{\omega/2}\rangle \otimes |\Psi_N\rangle. \quad (8)$$

In a perfect Si-crystal neutron interferometer the wavefunction behind the first plate, acting as a beam splitter, is a linear superposition of the sub-beams belonging to the right (|I>) and the left path (|II>), which are laterally separated by several centimeters. The sub-beams are recombined at the third crystal plate and the wave function in forward direction then reads as $|\Psi_N\rangle \propto |I\rangle + |II\rangle$, where |I> and |II> only differ by an adjustable phase factor $e^{i\chi}$ ($\chi = -N_{\text{ps}}b_c\lambda D$, with the atom number density N_{ps} in the phase shifter plate, the coherent scattering length b_c , the neutron wavelength λ and the thickness of the phase shifter plate D). By rotating the plate, χ can be varied. This yields the well known sinusoidal intensity oscillations of the two beams emerging behind the interferometer, usually denoted as O- and H-beam [13].

In our experiment, only the beam in path II is exposed to the rf-field of frequency ω , resulting in a spin flip (see Fig. 4 (a)). Interacting with a time-dependent magnetic field, the total energy of the neutron is no longer conserved after the spin-flip [39, 40, 41, 42, 43, 44]. Photons of energy $\hbar\omega$ are exchanged with the rf-field.

The time-dependent entangled state, which emerges from a coherent superposition of |I> and |II>, is expressed as

$$|\Psi_{\text{tot}}\rangle = |\alpha_\omega\rangle \otimes |\alpha_{\omega/2}\rangle \otimes \frac{1}{\sqrt{2}} \left(|I\rangle \otimes |\uparrow\rangle + e^{i\omega t} e^{i\chi} |II\rangle \otimes e^{i\phi_1} |\downarrow\rangle \right), \quad (9)$$

for a more detailed description of the generation of $|\Psi_{\text{tot}}\rangle$ see [45].

The effect of the first rf-flipper, placed inside the interferometer (path II), is described by the unitary operator $\hat{U}(\phi_I)$, which induces a spinor rotation from $|\uparrow\rangle$ to $|\downarrow\rangle$, we denoted $\hat{U}(\phi_I)|\uparrow\rangle = e^{i\phi_1}|\downarrow\rangle$. The rotation axis encloses an angle ϕ_I with the $\hat{\mathbf{x}}$ -direction, in the rotating frame, and is determined by the oscillating magnetic field $B^{(1)} = B_{\text{rf}}^{(\omega)} \cos(\omega t + \phi_I) \cdot \hat{\mathbf{y}}$. Formally one can insert a unity operator, given by

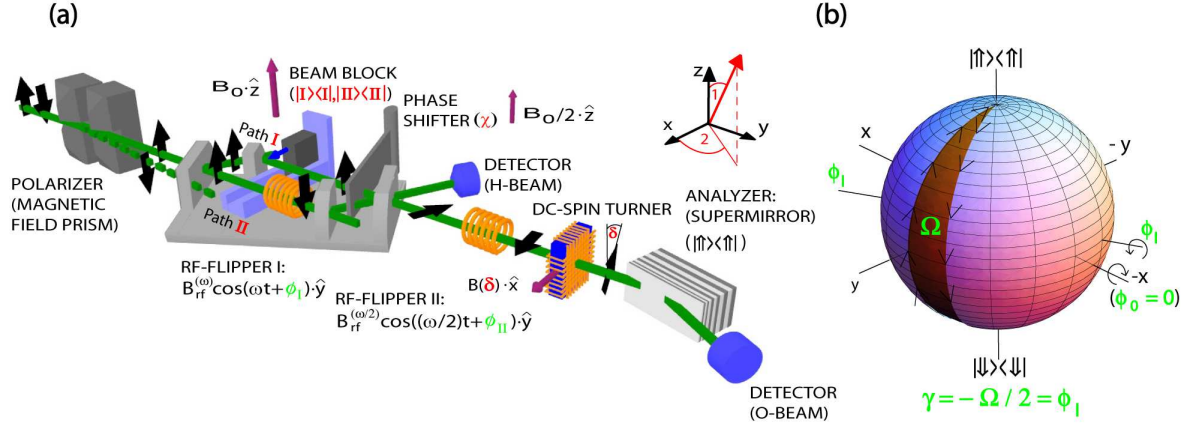


Figure 4. (a) The experimental apparatus for observation of geometric phase. The spin state acquires a geometric phase γ during the interaction with the two rf-fields and is flipped twice. Finally, the spin is rotated by an angle $\delta = \pi/2$ (in the $\hat{\mathbf{x}}, \hat{\mathbf{z}}$ plane), by a dc-spin turner, for a polarization analysis and count rate detection. (b) The Bloch-sphere description depicts the acquired geometric phase given by minus half the solid angle depending on the phase ϕ_I of the rf-field. The effect of the beam block is explained in Section 4.

$\mathbb{1} = \hat{U}^\dagger(\phi_0)\hat{U}(\phi_0)$, yielding

$$\hat{U}(\phi_I)|\uparrow\rangle = \underbrace{\hat{U}(\phi_I)\hat{U}^\dagger(\phi_0)}_{\mathbb{1}}\hat{U}(\phi_0)|\uparrow\rangle = e^{i\gamma}|\downarrow\rangle, \quad (10)$$

where $\hat{U}(\phi_0)$ can be interpreted as a rotation from $|\uparrow\rangle$ to $|\downarrow\rangle$, with the $\hat{\mathbf{x}}$ -direction being the rotation axis ($\phi_0 = 0$), and $\hat{U}^\dagger(\phi_0)$ describes a rotation about the same axis back to the initial state $|\uparrow\rangle$. Consequently, $\hat{U}(\phi_I)\hat{U}^\dagger(\phi_0)$ can be identified to induce the geometric phase γ , along the reversed evolution path characterized by ϕ_0 ($|\downarrow\rangle$ to $|\uparrow\rangle$), followed by another path determined by ϕ_I ($|\uparrow\rangle$ to $|\downarrow\rangle$), see Fig. 4 (b). In the rotating frame of reference [46] the two semi-great circles enclose an angle ϕ_I and the solid angle $\Omega = -2\phi_I$, yielding a pure geometric phase

$$\gamma = -\Omega/2 = \phi_I, \quad (11)$$

which is depicted in Fig. 4 (b). The entangled state, as described in [22], is represented by

$$|\Psi_{\text{Exp}}(\gamma)\rangle = \frac{1}{\sqrt{2}}\left(|\text{I}\rangle \otimes |\uparrow\rangle + |\text{II}\rangle \otimes e^{i\gamma}|\downarrow\rangle\right), \quad (12)$$

including the geometric phase $\gamma = \phi_I$.

3.1. Experimental Setup

As in a previous experiment [45], the spin in path $|\text{II}\rangle$ is flipped by a rf-flipper, which requires two magnetic fields: A static field $B_0 \cdot \hat{\mathbf{z}}$ and a perpendicular oscillating field

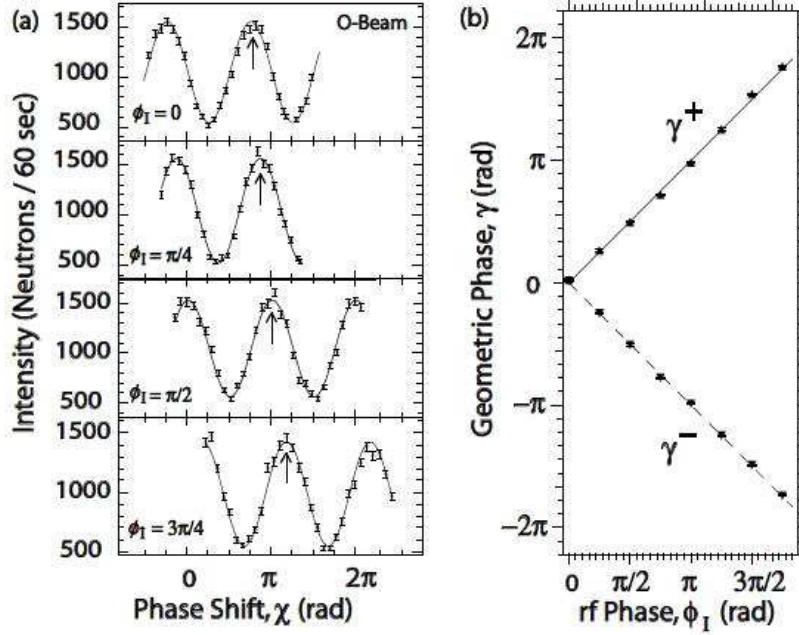


Figure 5. (a) Typical interference patterns of the O-beam, when rotating the phase shifter plate (χ). (b) A phase shift occurs by varying ϕ_I determining the geometric phase γ . The sign of the geometric phase γ^\pm depends on the chosen initial polarization.

$B^{(1)} = B_{\text{rf}}^{(\omega)} \cos(\omega t + \phi_I) \cdot \hat{y}$ satisfying the amplitude and frequency resonance condition

$$B_{\text{rf}}^{(\omega)} = \frac{\pi \hbar}{\tau |\mu|} \quad \text{and} \quad \omega = \frac{2|\mu|B_0}{\hbar} \left(1 + \frac{B_1^2}{16B_0^2}\right), \quad (13)$$

where μ is the magnetic moment of the neutron and τ denotes the time the neutron is exposed to the rf-field. The second term in ω is due to the Bloch-Siegert shift [47]. The oscillating field is produced by a water-cooled rf-coil with a length of 2 cm, operating at a frequency of $\omega/2\pi = 58$ kHz. The static field is provided by a uniform magnetic guide field $B_0^{(\omega)} \sim 2$ mT, produced by a pair of water-cooled Helmholtz coils.

The O-beam passes the second rf-flipper, operating at $\omega/2\pi = 29$ kHz, which is half the frequency of the first rf-flipper. The oscillating field is denoted as $B_{\text{rf}}^{(\omega/2)} \cos((\omega/2)t + \phi_{II}) \cdot \hat{y}$, and the strength of the guide field was tuned to $B_0^{(\omega/2)} \sim 1$ mT in order to satisfy the frequency resonance condition. This flipper compensates the energy difference between the components from the two interfering paths, by absorption and emission of photons of energy $E = \hbar\omega/2$. By choosing a frequency of $\omega/2$ for the second rf-flipper, the time-dependence of the state vector is eliminated since both components acquire a phase $e^{\pm i\omega/2(t+T)}$, depending on the spin orientation. Only a constant phase offset of $e^{\omega T}$, where T is the propagation time between the centre of the first and second flipper coil, remains in the stationary state vector. This phase contribution, together with a dynamical phase contribution, resulting from Larmor precession within the guide field regions $B_0^{(\omega)}$ and $B_0^{(\omega/2)}$ (pointing in $+\hat{z}$ -direction), are omitted here because they remain constant during the entire experiment. Finally,

the spin is rotated by an angle $\delta = \pi/2$ (in the $\hat{\mathbf{x}}, \hat{\mathbf{z}}$ plane) with a static field spin-turner, and analyzed due to the spin dependent reflection within a Co-Ti multi-layer supermirror along the $\hat{\mathbf{z}}$ -direction. Intensity oscillations in forward direction (O-beam) are plotted in Fig. 5 (a).

In a non-dispersive arrangement of the monochromator and the interferometer crystal the angular separation can be used such that only the spin-up (or spin-down) component fulfils the Bragg-condition at the first interferometer plate (beam splitter). Therefore it is possible to invert the initial polarization simply by rotating the interferometer by a few seconds of arc, which is expected to lead to an inversion of the geometric phase. Figure 5(b) shows a plot of the geometric phase $\Delta\gamma^\pm$ versus ϕ_{I} , with $\phi_{\text{II}} = 0$. As expected, the slope s is positive for initial spin up orientation ($s = 1.007(8)$), and negative for the spin down case ($s = -0.997(5)$), as predicted in Eq.(11)

4. Geometric phase effects on a spin-path entangled System

In this Section the influence of the geometric phase on a Bell measurement [48], expressed by the Clauser-Horne-Shimony-Holt (CHSH) [49] inequality, as proposed in [22] is discussed. Following the notation given in [22], the neutron's wavefunction is defined via tensor product of two Hilbert spaces: One Hilbert space is spanned by two possible paths in the interferometer given by $|I\rangle$ and $|II\rangle$; the other one by spin-up and spin-down eigenstates, denoted as $|\uparrow\rangle$ and $|\downarrow\rangle$, with respect to a quantization axis along a static magnetic field. For this experiment we focus on the neutron part of Eq.(9) and omit all phases but the geometric phase γ :

$$|\Psi_{\text{N}}(\gamma)\rangle = \frac{1}{\sqrt{2}} \left(|I\rangle \otimes |\uparrow\rangle + |II\rangle \otimes e^{i\gamma} |\downarrow\rangle \right). \quad (14)$$

As in common Bell experiments a joint measurement for spin and path is performed, thereby applying the projection operators for the path

$$\hat{P}_{\pm}^{\text{P}}(\boldsymbol{\alpha}) = |\pm \boldsymbol{\alpha}\rangle \langle \pm \boldsymbol{\alpha}|, \quad (15)$$

with

$$|+ \boldsymbol{\alpha}\rangle = \cos \frac{\alpha_1}{2} |I\rangle + e^{i\alpha_2} \sin \frac{\alpha_1}{2} |II\rangle \quad \text{and} \quad |- \boldsymbol{\alpha}\rangle = -\sin \frac{\alpha_1}{2} |I\rangle + e^{i\alpha_2} \cos \frac{\alpha_1}{2} |II\rangle, \quad (16)$$

where α_1 denotes the polar angle and α_2 the azimuthal angle for the path. This is done in analogous manner for the spin subspace with β_1 as the polar angle and β_2 as the azimuthal angle for the spin. Introducing the observables

$$\hat{A}^{\text{P}}(\boldsymbol{\alpha}) = \hat{P}_{+}^{\text{P}}(\boldsymbol{\alpha}) - \hat{P}_{-}^{\text{P}}(\boldsymbol{\alpha}) \quad \text{and} \quad \hat{B}^{\text{S}}(\boldsymbol{\beta}) = \hat{P}_{+}^{\text{S}}(\boldsymbol{\beta}) - \hat{P}_{-}^{\text{S}}(\boldsymbol{\beta}) \quad (17)$$

one can define an expectation value for a joint measurement of spin and path along the directions $\boldsymbol{\alpha}$ and $\boldsymbol{\beta}$

$$\begin{aligned} E(\boldsymbol{\alpha}, \boldsymbol{\beta}) &= \langle \Psi | \hat{A}^{\text{P}}(\boldsymbol{\alpha}) \otimes \hat{B}^{\text{S}}(\boldsymbol{\beta}) | \Psi \rangle = -\cos \alpha_1 \cos \beta_1 - \cos(\alpha_2 - \beta_2 + \gamma) \sin \alpha_1 \sin \beta_1 \quad (18) \\ &= -\cos(\alpha_1 - \beta_1) \quad \text{for} \quad (\alpha_2 - \beta_2) = -\gamma. \end{aligned}$$

Next, a Bell-like inequality in CHSH-formalism [49] is introduced, consisting of four expectation values with the associated directions α , α' and β , β' for joint measurements of spin and path, respectively

$$S(\alpha, \alpha', \beta, \beta', \gamma) = |E(\alpha, \beta) - E(\alpha, \beta') + E(\alpha', \beta) + E(\alpha', \beta')| \quad (19)$$

Without loss of generality one angle can be eliminated by setting, e.g., $\alpha = 0$ ($\alpha_1 = \alpha_2 = 0$), which gives

$$S(\alpha', \beta, \beta', \gamma) = \left| -\sin \alpha'_1 \left(\cos(\alpha'_2 - \beta_2 - \gamma) \sin \beta_1 + \cos(\alpha'_2 - \beta'_2 - \gamma) \sin \beta'_1 \right) - \cos \alpha'_1 (\cos \beta_1 + \cos \beta'_1) - \cos \beta_1 + \cos \beta'_1 \right|. \quad (20)$$

The boundary of Eq.(19) is given by the value 2 for any noncontextual hidden-variable theories [50]. Keeping the polar angles α'_1 , β_1 and β'_1 constant at the usual Bell angles $\alpha'_1 = \frac{\pi}{2}$, $\beta_1 = \frac{\pi}{4}$, $\beta'_1 = \frac{3\pi}{4}$ (and azimuthal parts fixed at $\alpha'_2 = \beta_2 = \beta'_2 = 0$) reduces S to

$$S(\gamma) = |-\sqrt{2} - \sqrt{2} \cos \gamma|, \quad (21)$$

where the familiar maximum value of $2\sqrt{2}$ is reached for $\gamma = 0$. For $\gamma = \pi$ the value of S approaches zero.

4.1. Polar Angle Adjustment

Here we consider the case when the azimuthal angles are kept constant, e.g., $\alpha'_2 = \beta_2 = \beta'_2 = 0$ ($\alpha_2 = 0$), which is depicted in Fig.6 The S -function reads as

$$S(\alpha'_1, \beta_1, \beta'_1, \gamma) = \left| -\sin \alpha'_1 \left(\cos \gamma \sin \beta_1 + \cos \gamma \sin \beta'_1 \right) - \cos \alpha'_1 (\cos \beta_1 + \cos \beta'_1) - \cos \beta_1 + \cos \beta'_1 \right|. \quad (22)$$

The polar Bell angles β_1 , β'_1 and α'_1 ($\alpha_1 = 0$), yielding a maximum S -value, can be determined, with respect to the geometric phase γ , by calculating the partial derivatives

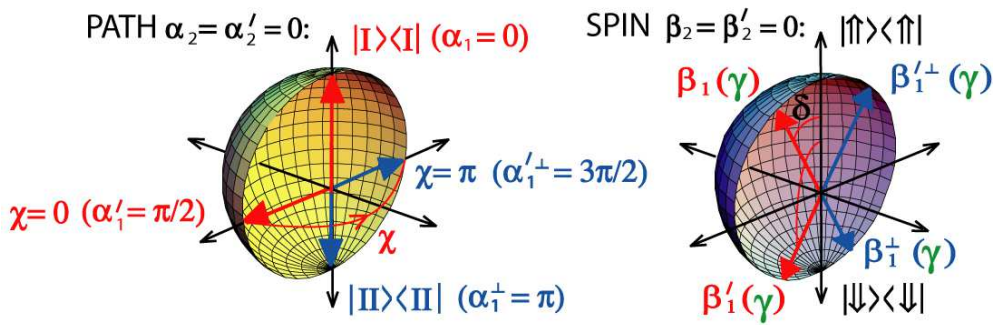


Figure 6. Bloch-sphere description includes the measurement settings of α and $\beta(\delta)$, determining the projection operators, used for joint measurement of spin and path. α is tuned by a combination of the phase shifter (χ) and the beam block, and β is adjusted by the angle δ .

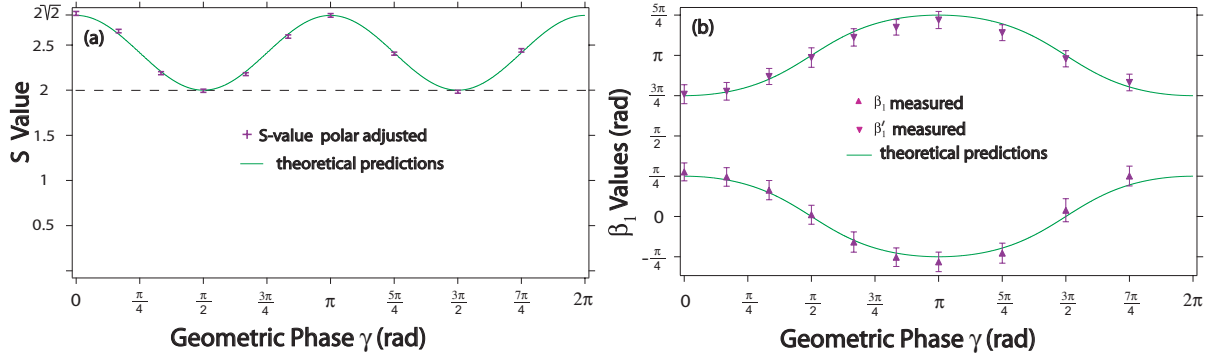


Figure 7. (a) Polar adjusted S -values versus geometric phase γ with adapted Bell angles (β_1 and β'_1) according to the geometric phase γ . (b) the corresponding modified Bell angles are plotted versus the geometric phase γ .

(the extremum condition) of S in Eq.(22)(see [22] for more elaborated deduction): The solutions are given by

$$\beta_1 = \arctan(\cos \gamma), \quad \beta'_1 = \pi - \beta_1 \quad \text{and} \quad \alpha'_1 = \frac{\pi}{2}, \quad (23)$$

which are plotted in Fig.7(b) (denoted as theoretical predictions). With these angles the maximal S decreases from $S = 2\sqrt{2}$ for $\gamma : 0 \rightarrow \frac{\pi}{2}$ and touches at $\gamma = \frac{\pi}{2}$ even the limit of the CHSH inequality $S = 2$. Within the interval $\gamma : \frac{\pi}{2} \rightarrow \pi$ the value of S increases again and returns to the familiar value $S = 2\sqrt{2}$ at $\gamma = \pi$.

Experimentally, the probabilities of joint (projective) measurements are proportional to the following count rates N_{ij} with ($i, j = +, -$), detected after path (α) and spin (β) manipulation:

$$E(\alpha, \beta) = \frac{N_{++}(\alpha, \beta) - N_{+-}(\alpha, \beta) - N_{-+}(\alpha, \beta) + N_{--}(\alpha, \beta)}{N_{++}(\alpha, \beta) + N_{+-}(\alpha, \beta) + N_{-+}(\alpha, \beta) + N_{--}(\alpha, \beta)}, \quad (24)$$

with for example

$$N_{++}(\alpha, \beta) = N_{++}(\alpha, (\beta_1, 0)) \propto \langle \Psi_N(\gamma) | \hat{P}_+^P(\alpha) \otimes \hat{P}_+^S(\beta_1, 0) | \Psi_N(\gamma) \rangle \quad (25)$$

In the case of $N_{+-}(\alpha, \beta)$ the count rate is given by $N_{++}(\alpha, (\beta_1^\perp, 0))$, where $\beta_1^\perp = \beta_1 + \pi$. The procedure is applied to the count rates $N_{+-}(\alpha, \beta)$ and $N_{--}(\alpha, \beta)$. With these expectation values S can be calculated as defined in Eq.(19).

Projective measurements are performed on parallel planes defined by $\alpha_2 = \alpha'_2 = \beta_2 = \beta'_2 = 0$. For the path measurement the directions are given by $\alpha : \alpha_1 = 0, \alpha_2 = 0$, and $\alpha' : \alpha'_1 = \pi/2, \alpha'_2 = 0$.

The angle α , which corresponds to $+\hat{z}$ (and $-\hat{z}$ for $\alpha_1^\perp = \alpha_1 + \pi = \pi, \alpha_2 = 0$) is achieved by the use of a beam block which is inserted to stop beam II (I) in order to measure along $+\hat{z}$ (and $-\hat{z}$). The corresponding operators are given by

$$\begin{aligned} \hat{P}_{+z}^P(\alpha_1 = 0, \alpha_2 = 0) &= |I\rangle\langle I| \\ \hat{P}_{-z}^P(\alpha_1^\perp = \pi, \alpha_2 = 0) &= |II\rangle\langle II|, \end{aligned} \quad (26)$$

The angle α' is set by a superposition of equal portions of $|I\rangle$ and $|II\rangle$, represented on the equator of the Bloch sphere. The interferograms are achieved by a rotation of the phase shifter plate, associated with a variation of the path phase χ . All path scans are repeated at different values of the spin analysis direction δ in order to determine β_1 and β'_1 for a maximal violation of the Bell-like CHSH inequality. The projective measurement for $\alpha'_1 = \pi/2, \alpha'_2 = 0$ corresponds to a phase shifter position of $\chi = 0$ (and $\alpha'_1{}^\perp = \alpha'_1 + \pi = 3\pi/2, \alpha'_2 = 0$ to $\chi = \pi$). Projection operators read as

$$\hat{P}_{+x}^P(\alpha'_1 = \frac{\pi}{2}, \alpha'_2 = 0) = \frac{1}{2} \left((|I\rangle + |II\rangle)(\langle I| + \langle II|) \right) \quad (27)$$

$$\hat{P}_{-x}^P(\alpha'_1{}^\perp = \frac{3\pi}{2}, \alpha'_2 = 0) = \frac{1}{2} \left((|I\rangle - |II\rangle)(\langle I| - \langle II|) \right). \quad (28)$$

Using the measurement curves from Eq.(26) and Eq.(27), the S -value is calculated according to Eq.(19) as a function of the parameters β_1 and β'_1 , which are varied independently. The local maximum of the $S(\beta'_1, \beta_1)$ is determined numerically and plotted in Fig. 7 (a), with the corresponding values for β_1 and β'_1 in Fig. 7 (b).

4.2. Azimuthal Angle Adjustment

Next we discuss the situation where the standard maximal value $S = 2\sqrt{2}$ can be achieved by keeping the polar angles α'_1 , β_1 and β'_1 constant at the Bell angles $\alpha'_1 = \frac{\pi}{2}$, $\beta_1 = \frac{\pi}{4}$, $\beta'_1 = \frac{3\pi}{4}$, ($\alpha_1 = 0$), while the azimuthal parts, α'_2 , β_2 and β'_2 ($\alpha_2 = 0$), are varied. A Bloch sphere description of this configuration can be seen in Fig. 8. The corresponding S function is denoted as

$$S(\alpha'_2, \beta_2, \beta'_2, \gamma) = \left| -\sqrt{2} - \frac{\sqrt{2}}{2} \left(\cos(\alpha'_2 - \beta_2 - \gamma) + \cos(\alpha'_2 - \beta'_2 - \gamma) \right) \right|. \quad (29)$$

The maximum value $2\sqrt{2}$ is reached for

$$\beta_2 = \beta'_2, \quad \text{and} \quad \alpha'_2 - \beta'_2 = \gamma \pmod{\pi}. \quad (30)$$

For convenience $\beta_2 = 0$ is chosen.

Experimentally the angle between the measurement planes is adjusted by one azimuthal angle (α'_2), which is deduced by phase shifter (χ) scans.

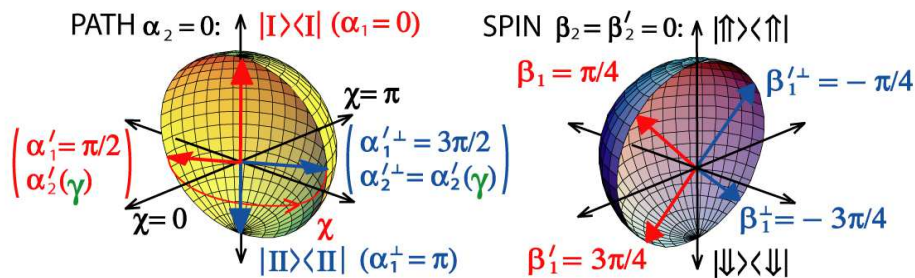


Figure 8. Bloch-sphere description includes the measurement settings of α and $\beta(\delta)$, determining the projection operators, used for joint measurement of spin and path.

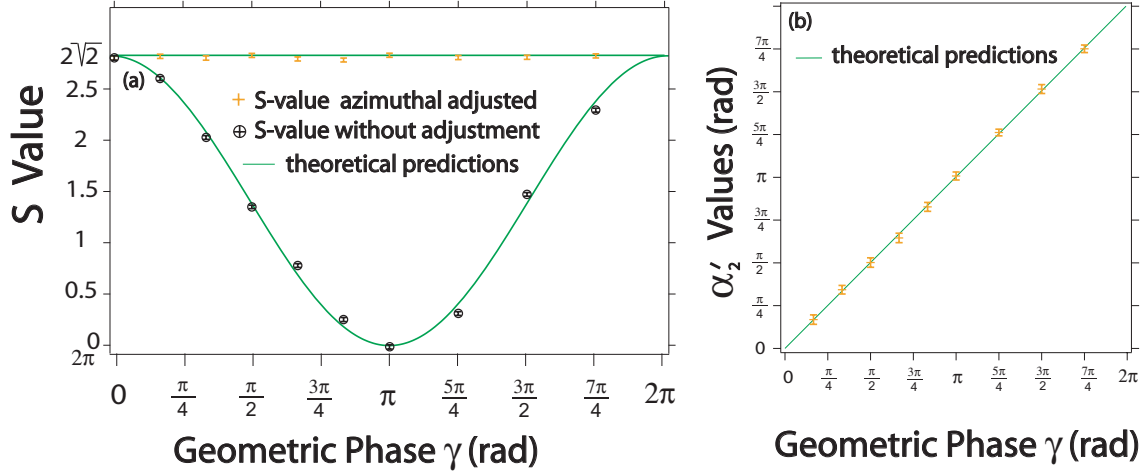


Figure 9. (Color online) (a) Azimuthal adjusted S -values versus geometric phase γ with balanced Bell angle (α'_2) according to the geometric phase γ , and without corrections. (b) the corresponding modified Bell angle is plotted versus the geometric phase γ .

For the spin measurement the directions are fixed and given by β : $\beta_1 = \pi/4$, $\beta_2 = 0$ and β' : $\beta'_1 = 3\pi/4$, $\beta'_2 = 0$ (together with $\beta_1^\perp = -3\pi/4$, $\beta_1'^\perp = -\pi/4$). For the projective path measurement the fixed directions read as $\alpha_1 = 0$ ($\alpha_1^\perp = \pi$), for measurements with beam block, and $\alpha'_1 = \pi/2$ ($\alpha_1'^\perp = 3\pi/2$). Phase shifter (χ) scans are performed in order to determine α'_2 for a maximal violation of the Bell-like CHSH inequality yielding $S = 2\sqrt{2}$.

As predicted by Eq.(30) the constant maximal S value of $2\sqrt{2}$ (see Fig.9(a)) is found for $\alpha'_2 = \gamma$, which is plotted in Fig.9(b). In Fig.9(a), the case is included where no corrections are applied to the Bell angles. According to Eq.(21) the familiar maximum value of $2\sqrt{2}$ is reached only for $\gamma = 0$, and at $\gamma = \pi$ the value of $S = 0$ is found.

This experiment demonstrates in particular, that a geometric phase in one subspace does not lead to a loss of entanglement. Two schemes, polar and azimuthal adjustment of the Bell angles, are realized, balancing the influence of the geometric phase. The former scheme yields a sinusoidal oscillation of the correlation function S , such that it varies in the range between 2 and $2\sqrt{2}$ and, therefore, always exceeds the boundary value 2 between quantum mechanical and noncontextual hidden-variable theories. The latter scheme results in a constant, maximal violation of the Bell-like CHSH inequality, where S remains $2\sqrt{2}$ independent of the value of the geometric phase γ .

5. Concluding remarks

Neutron optical experiments are used for studying characteristics of phases of geometric origin. First, non-additivity of the mixed state phase has been observed in a polarimetric experiment. Since the purity of quantum states in real experiments is always smaller

than 1, non-additivity is of importance in all applications of quantum phases. Thinking about phase gates, it means that the purity of the utilized quantum system has to be considered when inducing phases for further processing. Second, a technique for geometric phase generation has been established by means of a precise spin manipulation due to interaction with rf-fields, in an interferometric setup. Applying the formalism of the Jaynes-Cumming Hamiltonian to the patterns in the observed outgoing beam of the interferometer, we find good agreement between experiment and theory. This technique is also applied to phase manipulations of the spin subspace in a triple-entanglement experiment with neutrons, which will be topic of a forthcoming publication. Finally, the effect of the geometric phase on the entanglement of the system, has been analyzed in detail, using a Bell-like CHSH inequality. It is demonstrated, how the effects of the geometric phase on the outcome of a Bell measurement can be balanced by an appropriate change of Bell angles. Neutrons have proved to be a suitable quantum system for studying topological effects. Interferometric as well as polarimetric techniques will lead to further investigations, relevant for possible applications of the geometric phase. For instance, we are planning a polarimetric experiment, in which the geometric phase for non-unitary evolutions is considered.

5.1. Acknowledgments

This work has been supported by the Austrian Science Foundation, FWF (P21193-N20, P-17803-N02 and P- 20265). K.D.-R. would like to thank the FWF for funding her work by a Hertha Firnberg Position (T389-N16).

- [1] M. V. Berry. Quantal phase factors accompanying adiabatic changes. *Proc. R. Soc. Lond. A*, 392:45, 1984.
- [2] A. Tomita and R. Y. Chiao. Observation of Berry's topological phase by use of an optical fiber. *Phys. Rev. Lett.*, 57:937, 1986.
- [3] T. Bitter and D. Dubbers. Manifestation of Berry's topological phase in neutron spin rotation. *Phys. Rev. Lett.*, 59:251, 1987.
- [4] Y. Aharonov and J. S. Anandan. Phase change during a cyclic quantum evolution. *Phys. Rev. Lett.*, 58:1593, 1987.
- [5] J. Samuel and R. Bhandari. General setting for Berry's phase. *Phys. Rev. Lett.*, 60:2339, 1988.
- [6] N. Manini and F. Pistolesi. Off-diagonal geometric phases. *Phys. Rev. Lett.*, 85:3067, 2000.
- [7] A. Uhlmann. A gauge field governing parallel transport along mixed states. *Lett. Math. Phys.*, 21:229, 1991.
- [8] E. Sjöqvist, A. K. Pati, A. Ekert, J. S. Anandan, M. Ericsson, D. K. L. Oi, and V. Vedral. Geometric phases for mixed states in interferometry. *Phys. Rev. Lett.*, 85:2845, 2000.
- [9] J. Du, P. Zou, M. Shi, L. C. Kwek, J. W. Pan, C. H. Oh, A. Ekert, D. K. L. Oi, and M. Ericsson. Observation of geometric phases for mixed states using NMR interferometry. *Phys. Rev. Lett.*, 91:100403, 2003.
- [10] M. Ericsson, D. Achilles, J. T. Barreiro, D. Branning, N. A. Peters, and P. G. Kwiat. Measurement of geometric phase for mixed states using single photon interferometry. *Phys. Rev. Lett.*, 94:050401, 2005.
- [11] S. Filipp and E. Sjöqvist. Off-diagonal geometric phase for mixed states. *Phys. Rev. Lett.*, 90:050403, 2003.
- [12] S. Filipp and E. Sjöqvist. Off-diagonal generalization of the mixed-state geometric phase. *Phys. Rev. A*, 68:042112, 2003.
- [13] H. Rauch and S. A. Werner. *Neutron Interferometry*. Clarendon Press, Oxford, UK, 2000.
- [14] H. Rauch, W. Treimer, and U. Bonse. Test of a single crystal neutron interferometer. 47:369, 1974.
- [15] Y. Hasegawa, M. Zawisky, H. Rauch, and A. I. Ioffe. Geometric phase in coupled neutron interference loops. *Phys. Rev. A*, 53:2486, 1996.
- [16] S. Filipp, Y. Hasegawa, R. Loidl, and H. Rauch. Noncyclic geometric phase due to spatial evolution in a neutron interferometer. *Phys. Rev. A*, 72:021602(R), 2005.
- [17] A. G. Wagh, V. C. Rakhecha, P. Fischer, and A. I. Ioffe. Neutron interferometric observation of noncyclic phase. *Phys. Rev. Lett.*, 81:1992, 1998.
- [18] B. E. Allman, H. Kaiser, S. A. Werner, A. G. Wagh, V. C. Rakhecha, and J. Summhammer. Observation of geometric and dynamical phases by neutron interferometry. 56:4420, 1997.
- [19] M. A. Nielsen and I. L. Chuang. *Quantum Computation and Quantum Information*. Cambridge University Press, Cambridge, 2000.
- [20] P. J. Leek, J. M. Fink, A. Blais, R. Bianchetti, M. Göppl, J. M. Gambetta, D. I. Schuster, L. Frunzio, R. J. Schoelkopf, and A. Wallraff. Observation of Berry's phase in a solid-state qubit. *Science*, 318:1889, 2007.
- [21] S. Filipp, J. Klepp, Y. Hasegawa, C. Plonka-Spehr, U. Schmidt, P. Geltenbort, and H. Rauch. Experimental demonstration of the stability of Berry's phase for a spin-1/2 particle. *Phys. Rev. Lett.*, 102:030404, 2009.
- [22] R. A. Bertlmann, K. Durstberger, Y. Hasegawa, and B. C. Hiesmayr. Berry phase in entangled systems: A proposed experiment with single neutrons. *Phys. Rev. A*, 69:032112, 2004.
- [23] E. Sjöqvist. Geometric phase for entangled spin pairs. *Phys. Rev. A*, 62:022109, 2000.
- [24] D. M. Tong, L. C. Kwek, and C. H. Oh. Geometric phase for entangled states of two spin 1/2 particles in rotating magnetic field. *J. Phys. A*, 36(2):1149, 2003.
- [25] Y. Hasegawa, R. Loidl, G. Badurek, M. Baron, and H. Rauch. Violation of a Bell-like inequality in single-neutron interferometry. *Nature (London)*, 425:45, 2003.
- [26] Y. Hasegawa, R. Loidl, G. Badurek, S. Filipp, J. Klepp, and H. Rauch. Evidence for entanglement

- and full tomographic analysis of bell states in a single-neutron system. *Phys. Rev. A*, 76:052108, 2007.
- [27] J. Klepp, S. Sponar, Y. Hasegawa, E. Jericha, and G. Badurek. Noncyclic pancharatnam phase for mixed state $SU(2)$ evolution in neutron polarimetry. *Phys. Lett. A*, 342:48, 2005.
- [28] K. Singh, D. M. Tong, K. Basu, J. L. Chen, and J. F. Du. Geometric phases for nondegenerate and degenerate mixed states. *Phys. Rev. A*, 67:032106, 2003.
- [29] J. Klepp, S. Sponar, S. Filipp, M. Lettner, G. Badurek, and Y. Hasegawa. Observation of nonadditive mixed-state phases with polarized neutrons. *Phys. Rev. Lett.*, 101:150404, 2008.
- [30] J. Klepp, S. Sponar, S. Filipp, M. Lettner, G. Badurek, and Y. Hasegawa. Nonadditive mixed state phases in neutron optics. In *Foundations of Probability and Physics - 5*, page 314, Melville, New York, USA, 2009. American Institute of Physics.
- [31] S. Pancharatnam. Generalized theory of interference, and its applications. *Proc. Indian Acad. Sci.*, 44:247, 1956.
- [32] A. G. Wagh and V. C. Rakhecha. On measuring the Pancharatnam phase. II. $SU(2)$ polarimetry. *Phys. Lett. A*, 197:112, 1995.
- [33] P. Larsson and E. Sjöqvist. Noncyclic mixed state phase in $SU(2)$ polarimetry. *Phys. Lett. A*, 315:12, 2003.
- [34] R. A. Bertlmann, K. Durstberger, and Y. Hasegawa. Decoherence modes of entangled qubits within neutron interferometry. *Phys. Rev. A*, 73:022111, 2006.
- [35] E. T. Jaynes and F. W. Cummings. Comparison of quantum and semiclassical radiation theories with application to the beam maser. *Proc. IEEE*, 51:89, 1963.
- [36] B. W. Shore and P. L. Knight. Topical review of the Jaynes-Cummings model. *J. Mod. Optics*, 40:1195, 1993.
- [37] E. Muskat, D. Dubbers, and O. Schärpf. Dressed neutrons. *Phys. Rev. Lett.*, 58:2047, 1987.
- [38] C. Cohen-Tannoudji and S. Haroche. Interprétation quantique des diverses résonances observées lors de la diffusion de photons optiques et de radiofréquence par un atome. *J. Phys. (Paris)*, 30:125, 1969.
- [39] B. Alefeld, G. Badurek, and H. Rauch. Observation of the neutron magnetic resonance energy shift. *Z. Phys. B*, 41:231, 1981.
- [40] R. Gähler and R. Golub. A neutron resonance spin echo spectrometer for quasi-elastic and inelastic scattering. *Phys. Lett. A*, 43:123, 1987.
- [41] J. Summhammer. Coherent multiphoton exchange between a neutron and an oscillating magnetic field. *Phys. Rev. A*, 47:556, 1993.
- [42] R. Golub, R. Gähler, and T. Keller. A plane wave approach to particle beam magnetic resonance. *Am. J. Phys.*, 62:9, 1994.
- [43] J. Summhammer, K. A. Hamacher, H. Kaiser, H. Weinfurter, D. L. Jacobson, and S. A. Werner. Multiphoton exchange amplitudes observed by neutron interferometry. *Phys. Rev. Lett.*, 75:3206, 1995.
- [44] S. V. Grigoriev, W. H. Kraan, and M. T. Rekveldt. Four-wave neutron-resonance spin echo. *Phys. Rev. A*, 69:043615, 2004.
- [45] S. Sponar, J. Klepp, R. Loidl, S. Filipp, G. Badurek, Y. Hasegawa, and H. Rauch. Coherent energy manipulation in single-neutron interferometry. *Phys. Rev. A*, 78:061604(R), 2008.
- [46] D. Suter, K. T. Mueller, and A. Pines. Study of the Aharonov-Anandan quantum phase by NMR interferometry. *Phys. Rev. Lett.*, 60:1218, 1988.
- [47] F. Bloch and A. Siegert. Magnetic resonance for nonrotating fields. *Phys. Rev.*, 57(6):522, 1940.
- [48] J. S. Bell. On the Einstein-Podolsky-Rosen paradox. *Physics (Long Island City, N. Y.)*, 1(3):195, 1964.
- [49] J. F. Clauser, M. A. Horne, A. Shimony, and R. A. Holt. Proposed experiment to test local hidden-variable theories. *Phys. Rev. Lett.*, 23(15):880, 1969.
- [50] S. Basu, S. Bandyopadhyay, G. Kar, and D. Home. Bells inequality for a single spin-1/2 particle and quantum contextuality. *Phys. Lett. A*, 279:281, 2001.